JOURNAL OF SOLID STATE CHEMISTRY 99, 226–242 (1992)

The Incommensurately Modulated $(1 - x)Ta_2O_5 \cdot xWO_3$, $0 \leq x \leq 0.267$ Solid Solution

SIEGBERT SCHMID,* RAY L. WITHERS, AND JOHN G. THOMPSON

Research School of Chemistry, Australian National University, GPO Box 4, Canberra, ACT 2601, Australia

Received November 1, 1991; in revised form January 17, 1992; accepted January 20, 1992

The phase $(1 - x)Ta_2O_5 \cdot WO_3$, $0 \leq x \leq 0.267$ has been studied by X-ray powder diffraction and transmission electron microscopy. It was previously described as an infinite series of anion-deficient, α-UO_3-type "line phases," with compositions resulting from intergrowths of different blocks made up by small numbers of α-UO_3-type cells. More correctly $(1 - x)Ta_2O_5 \cdot xWO_3$, $0 \leq x \leq 0.267$ is described as an incommensurately modulated structure with a linearly composition-dependent primary modulation wave-vector $\mathbf{q}_{prim.} = q\mathbf{b}^*$. The underlying orthorhombically distorted α-UO_3-type parent structure has space group symmetry $Cmmm$ ($\mathbf{a} \approx 6.20$–6.14, $\mathbf{b} \approx 3.66$, $\mathbf{c} \approx 3.89$–3.85 Å). Characteristic extinction conditions imply a superspace group symmetry of $P:Cmmm:s,-1,1$. The four previously reported crystal structures in the solid solution field are examined by means of apparent valence calculations. Crystal chemical reasons are proposed for the width of the composition range, $0 \leq x \leq 0.267$, observed for the title phase.

1. Introduction

Many crystalline solids, like all molecular systems, possess a unique chemical composition. Such conventional crystalline solids are also characterized by having an immutable chemical environment or coordination polyhedron for each distinct atom in the chemical formula. Less conceptually easy to rationalize, however, are the large number of (nonstoichiometric) solid solutions—particularly wide range, nonstoichiometric solid solutions—with their apparent implication of infinitely adaptive coordination polyhedra.

Into this latter category fall several fascinating systems whose stoichiometry can be written as MA_{3-x} and which can all be described as modulated variants of an average, α-UO_3-related parent structure (see Fig. 1). The modulation of this average, α-UO_3-type parent structure (whose periodicity can be either commensurate or incommensurate with respect to the underlying α-UO_3-type subcell) is due to the ordering of anion vacancies along the **b** direction of the α-UO_3-type subcell. The inevitable structural relaxation which accompanies such anion vacancy ordering leads to a change in the local cation coordination polyhedra from hexagonal bipyramidal (as in α-UO_3) to pentagonal bipyramidal and distorted octahedral. Examples include the α-UO_{3-x} system itself, the $Ta_2O_5 \cdot TaO_2F$ (mole ratios from 1.5 : 1 up to 15 : 1) system (*1*), the $ZrO_2 \cdot ZrF_4$ (in the vicinity of 35 mol.% ZrF_4) sys-

* To whom correspondence should be addressed.

0022-4596/92 $5.00

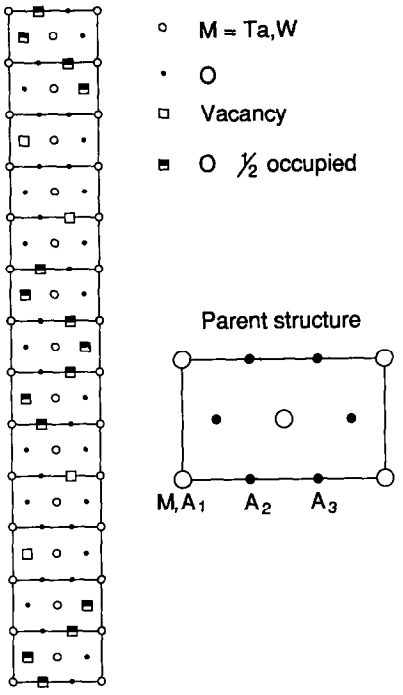

FIG. 1. Shows the (slightly orthorhombically distorted) α-UO_3-type underlying parent structure essentially responsible for the $(h, k, l, m = 0)^*$ reflections. The space group symmetry of this underlying parent structure is *Cmmm* ($\mathbf{a} \approx 6.14$, $\mathbf{b} \approx 3.66$, and $\mathbf{c} \approx 3.85$ Å) and there are four independent sites per primitive unit cell—*M* at 0,0,0 (Roth and Stephenson could not distinguish between Ta and W); A_1 at $0,0,\frac{1}{2}$; A_2 at $\frac{1}{3},0,0$, and A_3 at $\frac{2}{3},0,0$. Also shown is the compositional modulation of the parent structure of $Ta_{22}W_4O_{67}$ (see Fig. 1 of Ref. (*7*), i.e., and the A_2 and A_3 anion vacancy ordering scheme corresponding to the published structure.

tem (*2–4*), and the $Ta_2O_5 \cdot WO_3$ (from 0 to ~27 mol.% WO_3) system (*5–7*). The crystal chemistry underlying the existence and compositional ranges of these various systems is far from understood.

Of these systems $(1 - x)Ta_2O_5 \cdot xWO_3$, $0 \leq x \leq 0.267$ has been most extensively studied by X-ray powder and single crystal diffraction (*5, 6, 8–11*). This wide range, nonstoichiometric system was first discovered as a result of attempts to understand the structure of the low temperature polymorph of tantalum pentoxide (L-Ta_2O_5). The strong lines in the powder pattern could be indexed on the basis of an orthorhombically distorted, oxygen-deficient α-UO_3-type subcell with $a \approx 6.20$, $b \approx 3.66$, and $c \approx 3.89$ Å. However, numerous weak lines also occurred which were difficult to interpret unambiguously. As single crystals of L Ta_2O_5 could not be grown, attempts were made to stabilize this structure by adding other oxides. It was found that a variety of oxides could be used to "stabilize" phases very similar to L-Ta_2O_5, sometimes over quite a broad range of composition. In the case of WO_3, it was found that phases with subcells similar to L-Ta_2O_5 existed over a range of composition from pure Ta_2O_5 to ~26.67 mol.% WO_3, i.e., $11Ta_2O_5 \cdot 4WO_3$.

The seemingly chemically reasonable desire that there be as small a number of different coordination polyhedra as possible for each distinct ion in the chemical formula, e.g., Ta^{5+}, suggested that the modulation periodicity of any composition within this composition range should always be commensurate with respect to the underlying α-UO_3-type subcell. Thus, although no two-phase regions were ever found below the solidus for any composition from Ta_2O_5 to $11Ta_2O_5 \cdot 4WO_3$, the interpretation given was still in terms of a series of distinct line phases (albeit an "infinite" number thereof) rather than in terms of a continuous solid solution. The only reason given for not invoking a continuous solid solution was "the completely discontinuous shift of the **b** axis with composition" (*6*). The very definition of a **b** axis, however, assumes the existence of a superstructure and precludes the alternative possibility of an incommensurately modulated structure with continuously varying, composition-dependent, primary modulation wavevector. Very recently Williams *et al.* (*7*) have reported the results of an electron and powder X-ray diffraction study of various ternary L-Ta_2O_5-related phases including the $(1 - x)Ta_2O_5 \cdot xWO_3$,

$0 \leq x \leq 0.267$ system. They found a continuum of structures and suggested a model whereby the apparently continuously variable unit cell parameters could be interpreted in terms of an ordered intergrowth model. In order to test the hypothesis that the $(1 - x)Ta_2O_5 \cdot xWO_3$, $0 \leq x \leq 0.267$ system might best be described as a single incommensurately modulated structure with a composition-dependent primary modulation wave vector, we decided to undertake a systematic study of the phase relationships given by Roth and Stephenson (*5*).

Although there have been four published structure refinements (tours de force in their day) within the above stoichiometric range (*8–11*), none are very satisfactory chemically or crystallographically. For example, in each of these refinements there are always several nonbonded oxygen–oxygen contacts very much shorter (~0.3–0.5 Å) than the minimum chemically plausible distance of ~2.50 Å. In addition, bond length-bond valence calculations (see Section 5) do not give chemically plausible valences. Furthermore all of the refinements suffered from a high degree of parameter interaction and hence gave very large e.s.d's (~±0.2 Å) for the atomic coordinates and therefore for bond distances and angles. The desire to interpret this high degree of parameter interaction in terms of a modulation wave approach to structure refinement formed the second motivation for the present paper.

2. Experimental

2.1. Synthesis

Specimens were prepared from Ta_2O_5 (Koch-Light Laboratories Ltd., 99.9% pure) and WO_3 (Halewood Chemicals Ltd., 99.9% pure) at a range of compositions (0, 7.1, 18.8, 33.3, and 40.0 mol.% WO_3). Specimens were mechanically mixed, pressed into pellets, and heated for variable lengths of time at differing temperatures in sealed Pt tubes and on alumina supports in air. As L-Ta_2O_5 undergoes a phase transition at about 1360°C to an H-Ta_2O_5 phase the pure Ta_2O_5 specimens were heated at temperatures of 1050 and 1350°C for 88 and 92 hr, respectively. For the more WO_3-rich specimens it was necessary to use sealed platinum tubes in order to avoid loss of WO_3 during the reaction. The two specimens which are not in the two-phase region described by Roth and Stephenson were heated at 1600°C for 91 hr. The specimens in the two-phase region were heated at 1550, 1583, and 1600°C for 5, 7, and 3 days, respectively, in order to reach equilibrium.

2.2. XRD and Electron Diffraction

Specimens were examined by XRD using a Guinier–Hägg camera with monochromated Cu$K\alpha_1$ radiation. An internal standard of Si (NBS No. 640) was used to calibrate the measurement of XRD films for least-squares refinement of the unit cell dimensions and the magnitude of the modulation vector. The material was further studied on a JEOL 100CX transmission electron microscope.

3. Results and Discussion

3.1. Phase Relationships

The phase relationships were as reported by Stephenson and Roth except that the incommensurately modulated $(1 - x)Ta_2O_5 \cdot xWO_3$, $0 \leq x \leq 0.267$ phase field was found to be best treated as a single-phase "solid-solution." For specimens made with 26.7 < 50 mol.% WO_3 Ta_2WO_8 and $Ta_{22}W_4O_{67}$ were present in equilibrium.

3.2. Magnitude of the Modulation Vector

The magnitude of the modulation vector for each composition was determined from both X-ray powder diffraction and electron diffraction patterns. The electron diffraction patterns showed that the modulation vector lay directly along the **b*** direction, and that

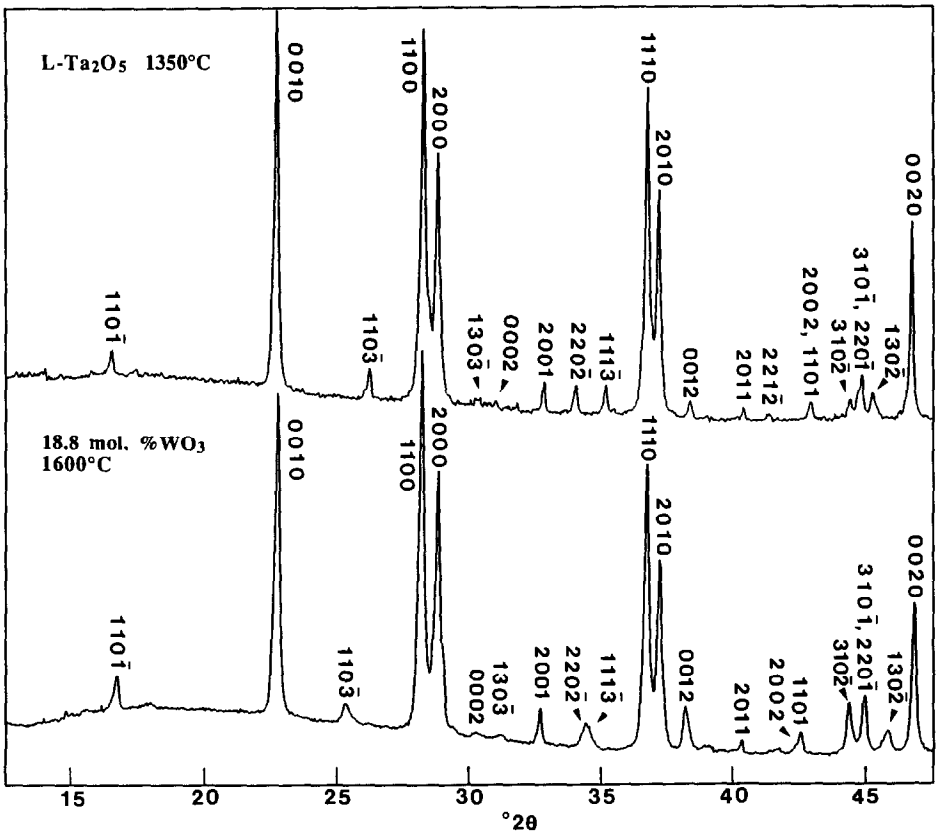

FIG. 2. Densitometer traces from XRD Guinier exposures (λ = 1.5406 Å) of 1350°C L-Ta_2O_5 and 1600°C 18.8 mol.% WO_3 specimens. A four-index notation $(h, k, l. m)$ has been used to index reflections. While the subcell reflections vary little in their position, the satellite reflections, notably 1, 1, 0, −3 and 1, 3, 0, −3 vary markedly.

it could be incommensurate with respect to **b*** (see Section 3.4).

Figure 2 shows densitometer traces from Guinier films of L-Ta_2O_5 at 1350°C and 18.8 mol.% WO_3 1600°C specimens. While the parent unit cell reflections $(h, k, l, m; m = 0)$* vary little between specimens the satellite reflections shift dramatically, particularly the higher-order harmonics, e.g. (1, 1, 0, −3)*; (1, 3, 0, −3)*; (0, 0, 0, 2)*; (1, 1, 1, −3)*; and (1, 3, 0, −2)*. From these films **q/b*** was accurately derived using the (1, 1, 0, −1)* and (1, 1, 0, −3)* satellite reflections (see Section 3.4 for indexing notation). Note that the so-called "**C**"-line which has often been used to determine the "**b**-axis multiplicity" corresponds to the {1, 1, 0, −3}* reflection in this four-index notation. The value of **q/b*** derived from the X-ray powder data, while in complete agreement with the value obtained from electron diffraction patterns, could be determined with higher precision. A plot of **q/b*** versus composition is given in Fig. 3. The magnitude of **q/b*** is linearly dependent on the composition, but the relation is more complex than in the case of $Zr_7O_9F_{10}$ (*4*). The experimental data for $(1 - x)Ta_2O_5 \cdot xWO_3$, $0 \leq x \leq 0.267$ fit the function $\mathbf{q} = (0.635 - 0.074x)\mathbf{b}^*$.

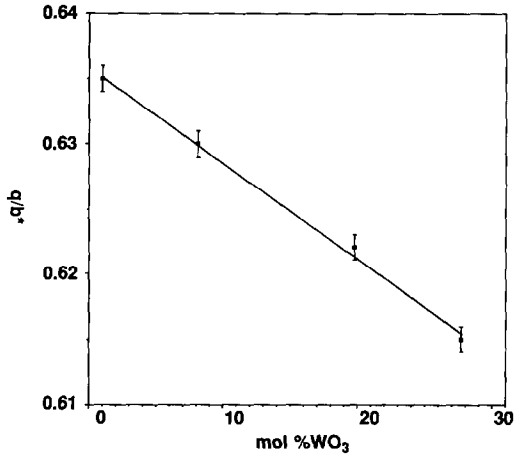

FIG. 3. Plot of XRD determined **q/b*** versus composition of $(1 - x)Ta_2O_5 \cdot xWO_3$ given in mol.% WO_3. Within experimental uncertainty there is a linear decrease of **q/b*** with increase of the WO_3 proportion.

3.3. Unit Cell Dimensions

The **C**-centered orthorhombic parent unit cell dimensions of the solid-solution field were determined using a least-squares refinement of parent unit cell data out to 47° 2θ for Cu$K\alpha_1$. These are presented in Fig. 4. There is a steady decrease in the **a** and **c** subcell dimensions as the mol.% of WO_3 increases whereas the subcell **b** dimension varies much less.

3.4. Electron Diffraction Patterns

Figure 5 shows (a) and (b) [100], (c) [001], and (d) [010] subcell zone-axis diffraction patterns typical of the $(1 - x)Ta_2O_5 \cdot xWO_3$, $0 \leq x \leq 0.267$ solid-solution field. A four-index notation $(h, k, l, m) = h\mathbf{a}^* + k\mathbf{b}^* + l\mathbf{c}^* + m\mathbf{q}$, where **a***, **b***, **c*** correspond to the cell dimensions of the reciprocal lattice of the underlying *Cmmm* parent structure (see Fig. 1) and where the primary modulation wavevector $\mathbf{q} \approx 0.615$–$0.635\ \mathbf{b}^*$, can be used to index any given reflection. In general, it is difficult to distinguish between parent and low order (i.e., $m = 1$ or 2) satellite reflections due to the large amplitude of these first few modulation harmonics. The intensity of the satellite reflections does, however, drop off sharply for $m > 2$ such that harmonics with $m > 9$ are never observed (see Fig. 6).

Note the characteristic satellite extinction condition $F(h, k, l, m)^* = 0$ unless $h + k = 2n$. This requires the underlying average structure to be **C**-centered. Note also the characteristic satellite extinction condition $F(0, k, l, m)^* = 0$ unless $m = 2n$ in Fig. 5a. The existence of such a characteristic satellite extinction condition requires the existence of the superspace group symmetry operation $\{\sigma_x|\mathbf{0}, \frac{1}{2}\}$ using the notation of Pérez-Mato *et al.* (*12*). The corresponding superspace group is thus $P : Cmmm : s, -1, 1$. Note also the characteristic diffuse intensity present in Figs. 5b and d. It appears to consist of diffuse sheets of intensity perpendicular to **c*** and running through the $\mathbf{G} \pm 0\mathbf{c}^*$ reciprocal space positions (horizontal arrows in Figs. 5b and d). The strong azimuthal intensity variation displayed by this

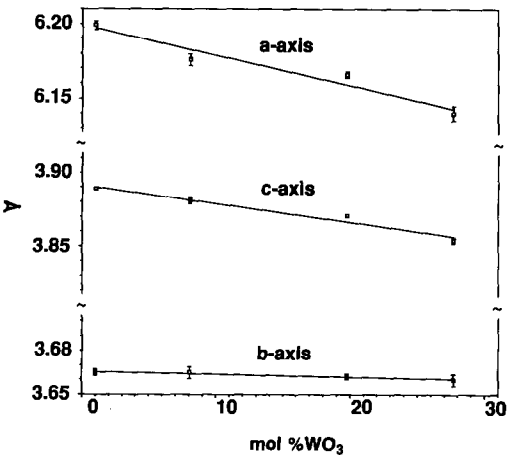

FIG. 4. Plot of refined parent unit cell dimensions versus composition of $(1 - x)Ta_2O_5 \cdot xWO_3$ given in mol.% WO_3. While there is a linear decrease in the **a** and **c** axis dimensions with increasing amount of WO_3 the **b** axis remains constant within experimental uncertainty.

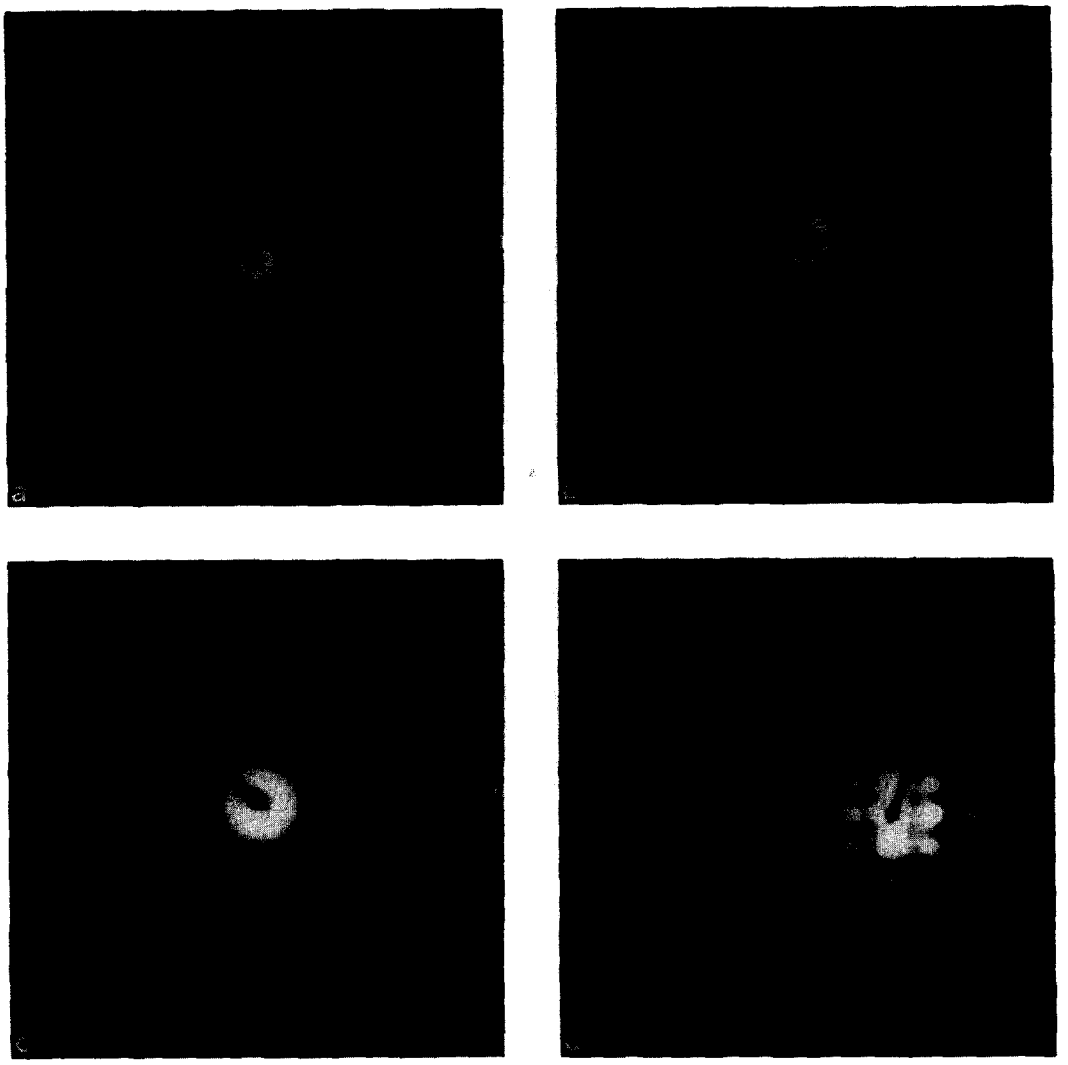

FIG. 5. Shows (a) and (b) [100], (c) [001] and (d) [010] subcell zone-axis electron diffraction patterns typical of the $(1 - x)Ta_2O_5 \cdot xWO_3$, $0 \leq x \leq 0.267$ solid solution field. Patterns (a) and (c) are Selected Area electron Diffraction Patterns (SADPs) while patterns (b) and (d) are Convergent Beam electron diffraction Patterns (CBPs). A four-index notation $(h, k, l, m) = h\mathbf{a}^* + k\mathbf{b}^* + l\mathbf{c}^* + m\mathbf{q}$, where $\mathbf{a}^*$, $\mathbf{b}^*$, $\mathbf{c}^*$ correspond to the cell dimensions of the reciprocal lattice of the underlying *Cmmm* parent structure and where the primary modulation wavevector $\mathbf{q} \approx 0.615$–$0.635\,\mathbf{b}^*$, can be used to index any given reflection. Note the characteristic diffuse intensity distribution arrowed in (b) and (d).

type of diffuse distribution in wider angle [100] (Fig. 5b) and [010] (Fig. 5d) Convergent Beam Patterns (CBPs) requires displacive shifts along the **c** axis to be responsible. This is discussed in more detail in Section 6. In spite of the very sharp subcell and satellite reflections, there is still clearly scope for compositional and displacive disorder. Note, however, that spot patterns show that there are really two diffuse

FIG. 6. Shows a blow-up of the central portion of a typical [001] zone axis SADP. The primary modulation wavevector $\mathbf{q} \sim 22/35\ \mathbf{b}^*$ and up to ninth-order harmonics are visible although only very weakly.

"sheets" split on either side of the $\mathbf{G} \pm 0\mathbf{c}^*$ planes (see Fig. 7) and that intensity shifts from the inner sheet to the outer sheet at large $\sin\theta/\lambda$. This effect suggests a size effect origin (*13, 14*) but further consideration of this complex diffuse distribution is beyond the scope of this paper.

4. A Modulation Wave Approach to the Structural Description of the $(1 - x)Ta_2O_5 \cdot xWO_3$, $0 \leq x \leq 0.267$ Solid-Solution Field

4.1. The Underlying Parent Structure

Given the continuous smooth variation of $\mathbf{q}/\mathbf{b}^*$ with composition and temperature, it is clear that any generally applicable crystallographic description of this system must be based upon a super-space group approach (*15*) rather than upon conventional crystallographic refinement at rational values of $\mathbf{q}/\mathbf{b}^*$. The underlying parent structure (see Fig. 1) can be taken to be a slightly orthorhombically distorted, oxygen-deficient, α-UO_3-type structure. This structure is essentially responsible for the $(h, k, l, m = 0)^*$ reflections. Its space group symmetry is *Cmmm* with $\mathbf{a} \approx 6.14$, $\mathbf{b} \approx 3.66$ and $\mathbf{c} \approx 3.85$ Å. There are four independent sites per primitive parent unit cell – M at 0, 0, 0; A_1 at 0, 0, $\frac{1}{2}$; A_2 at $\frac{1}{3}$, 0, 0; and A_3 at $\frac{2}{3}$, 0, 0. Stephenson and Roth (*8–11*) could not dis-

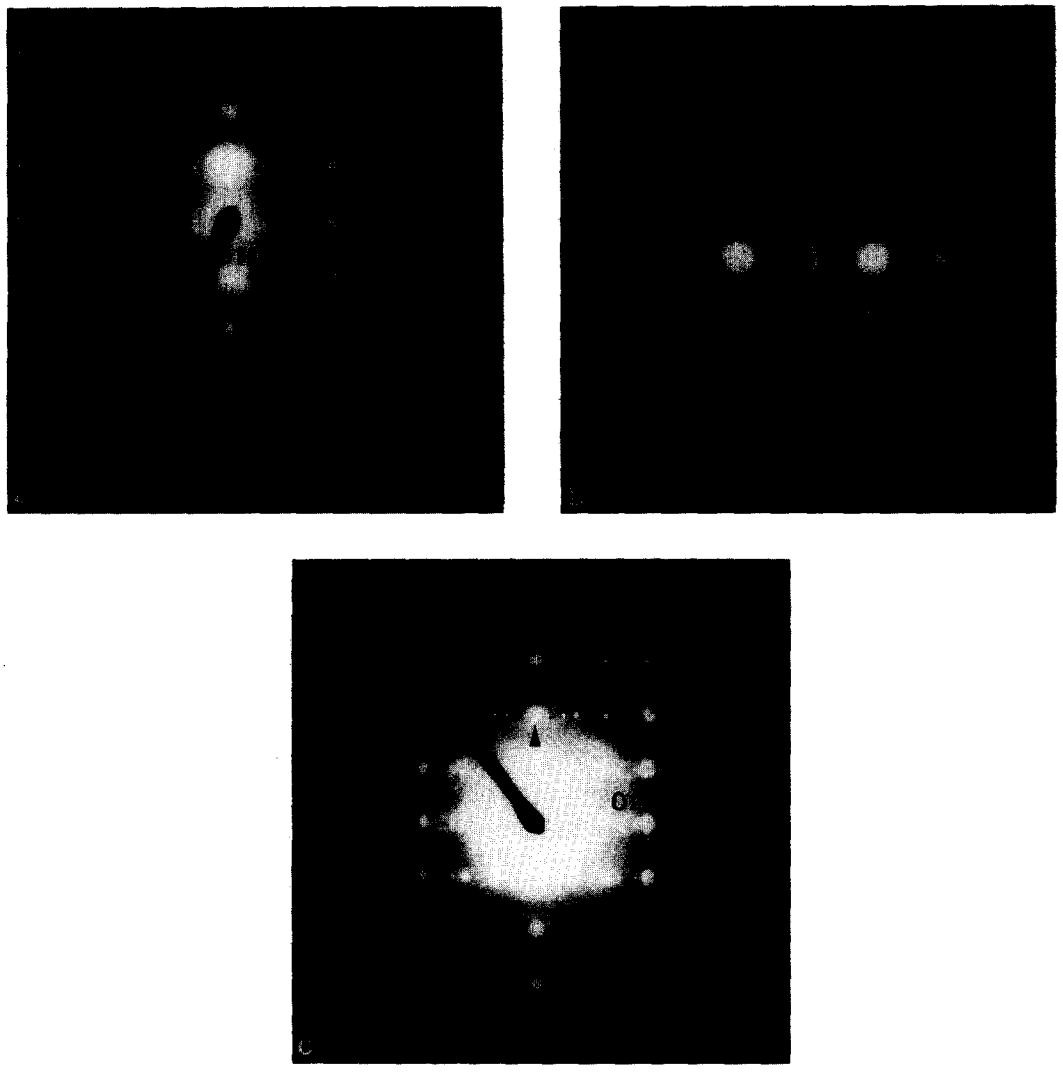

FIG. 7. SADPs showing the extremely characteristic "sheets" of diffuse intensity running perpendicular to $\mathbf{c}^*$ and narrowly split on either side of the $\mathbf{G}_{perp.} \pm 0\mathbf{c}^*$ planes of reciprocal space. Patterns (a) and (b) are superspace zone axis SADPs taken in the close vicinity of the [010] zone axis (Pattern (a) is tilted ~7° from [010] while keeping (0010)* excited. Pattern (b) is also tilted ~7° from [010] but this time (2000)* is kept excited). Pattern (c) is a conventional [100] zone axis SADP.

tinguish between Ta and W. Hence we will simply refer to cation sites as M. The average atomic scattering factors of the metal and anion sites, denoted $\underline{f}_M$, $\underline{f}_{A(1)}$, $\underline{f}_{A(2)}$, $\underline{f}_{A(3)}$, are necessarily composition-dependent, e.g., for a composition $(1 - x)Ta_2O_5 \cdot xWO_3 = Ta_{2-2x}W_xO_{5-2x}$,

$$\underline{f}_M = [(2 - 2x)/(2 - x)]\, f_{Ta} + [x/(2 - x)\, f_W$$
$$\underline{f}_{A(1)} = f_O;\ \underline{f}_{A(2)} = \underline{f}_{A(3)} = \underline{f}_A = [(3 - x)/(4 - 2x)]\, f_O$$

For example, $Ta_{22}W_4O_{67}$ has 41/52 of an anion at each of the A_2 and A_3 sites on average, i.e., the average atomic scattering fac-

tor of the A_2 and A_3 sites, $\underline{f}_{A(2)} = \underline{f}_{A(3)} = 41/52\, f_O$, while the anion site above the metal atoms A_1 always remains fully occupied, i.e., $\underline{f}_{A(1)} = f_O$ (see Sections 4.3 and 6).

4.2. *Defining the Modulations*

The deviation of the modulated structure from this basic structure can then be expressed in terms of compositional and displacive modulations as follows (*12*):

$$\delta f_\mu(\mathbf{T}) = \underline{f}_\mu \mathrm{Re}\left\{ \sum A_\mu(\mathbf{q}) \exp(2\pi i \mathbf{q}\cdot\mathbf{T}) \right\} \quad (1)$$

$$\mathbf{u}_\mu(\mathbf{T}) = \mathrm{Re}\left\{ \sum \mathbf{e}_\mu(\mathbf{q}) \exp(2\pi i \mathbf{q}\cdot\mathbf{T}) \right\}. \quad (2)$$

Here $\delta f_\mu(\mathbf{T})$ represents the deviation (from $\underline{f}_\mu$) of the atomic scattering factor of the μth atom in the **T**th parent primitive unit cell, while $\mathbf{u}_\mu(\mathbf{T})$ represents the atomic displacement away from its position in the parent structure ($\mathbf{r}_\mu + \mathbf{T}$) of the μth atom in the **T**th parent primitive unit cell. The compositional component of a modulation characterized by the modulation wavevector **q** is specified by its compositional eigenvector $A(\mathbf{q}) = (a_M, a_{A(1)}, a_{A(2)}, a_{A(3)})$, where the a_μ's are, in general, complex numbers, while the displacive component is specified by its displacement eigenvector $\mathbf{e}(\mathbf{q}) = (e_{Mx}, e_{My}, e_{Mz}; e_{A(1)x}, e_{A(1)y}, e_{A(1)z}; e_{A(2)x}, e_{A(2)y}, e_{A(2)z}; e_{A(3)x}, e_{A(3)y}, e_{A(3)z})$, where the $e_{\mu\alpha}$'s are again in general complex numbers representing the shifts of the μth atom along the αth (= **a**, **b**, or **c**) directions. If such modulations have non-zero amplitude, they will give rise to satellite reflections at $\mathbf{G} \pm m\mathbf{q}$, where **G** is a Bravais Lattice allowed reflection of the $\alpha - UO_3$-related parent structure. Note that displacive modulations with modulation wavevector **q** give rise to intensity not just at $\mathbf{G} \pm \mathbf{q}$ but at $\mathbf{G} \pm m\mathbf{q}$, where m is an integer.

Such modulations are characterized by their transformation properties under the space group symmetry operations belonging to the little group of the corresponding modulation wavevector (*16*). It is often the case that compositional and/or displacive modulations associated with specific modulation wavevectors transform according to a particular irreducible representation (see Table I) of the corresponding little cogroup, in this case $C_{2v} = \{E, C_{2y}, \sigma_x, \sigma_z\}$. The diffraction symmetry characteristic of this incommensurately modulated phase (see Fig. 5) imply that odd order harmonics transform with R_4 symmetry while even order harmonics transform with R_1 symmetry. The equivalent superspace group symmetry is $P:Cmmm:s,\text{-}1,1$. The characteristic satellite extinction condition observed at the [100] zone axis (see Fig. 5b) is a consequence of the superspace group symmetry operation $\{\sigma_x|\mathbf{0}, \frac{1}{2}\}$ using the notation of Pérez-Mato *et al.* (*12*). Complete specification of such a structure consists of determining the above parent structure plus the Atomic Modulation Functions (AMFs) (*12, 17*) describing the compositional fluctuations and displacive shifts away from this underlying parent structure as a function of $\mathbf{q}\cdot\mathbf{T}$, where **q** is the primary modulation wavevector $\approx 0.62\,\mathbf{b}^*$ and $\mathbf{T} = m\mathbf{a} + n\mathbf{b} + p\mathbf{c} + q\cdot\frac{1}{2}(\mathbf{a}+\mathbf{b})$ (m, n, p, q all integers) labels the different cells of the parent structure. The above super-space group severely constrains the form of these AMFs.

TABLE I

ONE-DIMENSIONAL IRREDUCIBLE REPRESENTATIONS OF *Cmmm* ASSOCIATED WITH THE $\mathbf{q}_{\text{prim.}} = q\mathbf{b}^*$ PRIMARY MODULATION WAVEVECTOR

	E	C_{2y}	σ_x	σ_z
R_1	1	1	1	1
R_2	1	1	−1	−1
R_3	1	−1	1	−1
R_4	1	−1	−1	1

4.3. The AMFs

The most general possible compositional AMFs describing the compositional deviation from the underlying parent structure defined above can then be written in the form

$$\delta f_M(\mathbf{T}) = \underline{f}_M \sum a_M(2m\mathbf{q}) \cos(2\pi \cdot 2m\mathbf{q} \cdot \mathbf{T} + 2m\phi)$$

$$\delta f_{A(1)}(\mathbf{T}) = \underline{f}_{A(1)} \sum a_{A(1)}(2m\mathbf{q}) \cos(2\pi \cdot 2m\mathbf{q} \cdot \mathbf{T} + 2m\phi)$$

$$\delta f_{A(2),A(3)}(\mathbf{T}) = \underline{f}_A \sum \{a_A(2m\mathbf{q}) \cos(2\pi \cdot 2m\mathbf{q} \cdot \mathbf{T} + 2m\phi) \pm a_A([2m + 1]\mathbf{q}) \cos(2\pi \cdot [2m + 1]\mathbf{q} \cdot \mathbf{T} - 90° + [2m + 1]\phi)\}, \quad (3)$$

where the summations are over m = 1, 2, 3, . . ., (we assume the average composition to be correct and hence there is no need to allow for the possibility of an $m = 0$ compositional wave) and where the + sign corresponds to the $A(2)$ site and the − sign to the $A(3)$ site in the latter expression. In practice, the anion site above the metal atoms must always remain occupied for obvious crystal chemical reasons and hence $a_{A(1)}(2m\mathbf{q})$ can always be put to zero for all m. There is therefore one compositional degree of freedom for odd order harmonics and two compositional degrees of freedom for even order harmonics. In practice, the atomic scattering factors of W and Ta for X-rays are too close to be distinguished so that the $a_M(2m\mathbf{q})$'s can not be refined. The global phase parameter, ϕ, can be chosen arbitrarily when $\mathbf{q}$ is incommensurate. When $\mathbf{q}$ is commensurate, however, the resultant conventional space group symmetry is dependent upon this global phase parameter.

The most general possible displacive AMFs describing the structural deviation from the underlying parent structure defined above can be written in the form:

$$\mathbf{u}_M(\mathbf{T}) = \sum \{\mathbf{a}\varepsilon_{Mx}([2m + 1]\mathbf{q}) \cos(2\pi \cdot [2m + 1]\mathbf{q} \cdot \mathbf{T} - 90° + [2m + 1]\phi + \mathbf{b}\varepsilon_{My}(2m\mathbf{q}) \cos(2\pi \cdot 2m\mathbf{q} \cdot \mathbf{T} - 90° + 2m\phi)\}$$

$$\mathbf{u}_{A(1)}(\mathbf{T}) = \sum \{\mathbf{a}\varepsilon_{A(1)x}([2m + 1]\mathbf{q}) \cos(2\pi \cdot [2m + 1]\mathbf{q} \cdot \mathbf{T} - 90° + [2m + 1]\phi) + \mathbf{b}\varepsilon_{A(1)y}(2m\mathbf{q}) \cos(2\pi \cdot 2m\mathbf{q} \cdot \mathbf{T} - 90° + 2m\phi)\}$$

$$\mathbf{u}_{A(2),A(3)}(\mathbf{T}) = \sum \{\pm\mathbf{a}\varepsilon_{Ax}(2m\mathbf{q}) \cos(2\pi \cdot 2m\mathbf{q} \cdot \mathbf{T} + 2m\phi) + \mathbf{b}\varepsilon_{Ay}(2m\mathbf{q}) \cos(2\pi \cdot 2m\mathbf{q} \cdot \mathbf{T} - 90° + 2m\phi) + \mathbf{a}\varepsilon_{Ax}([2m + 1]\mathbf{q}) \cos(2\pi \cdot [2m + 1]\mathbf{q} \cdot \mathbf{T} - 90° + [2m + 1]\phi \pm \mathbf{b}\varepsilon_{Ay}([2m + 1]\mathbf{q}) \cos(2\pi \cdot [2m + 1]\mathbf{q} \cdot \mathbf{T} + [2m + 1]\phi)\}, \quad (4),$$

where the summations are over m = 0, 1, 2, 3, . . ., and where the + sign corresponds to the $A(2)$ site and the − sign to the $A(3)$ site. There is one displacive degree of freedom for $m = 0$ and four displacive degrees of freedom for each other order of harmonic (i.e., $m \neq 0$) in addition to the global phase parameter. Note that an origin shift of $\mathbf{T}_0 = m\mathbf{a} + n\mathbf{b} + p\mathbf{c} + q \cdot \frac{1}{2}(\mathbf{a} + \mathbf{b})$ is equivalent to a change in ϕ of $-2\pi\ \mathbf{q} \cdot \mathbf{T}_0$.

4.4. Crystallographic Refinement Consequences

Given that the highest order harmonic ever visible in electron diffraction patterns from any composition within the stoichiometric range is $m = 9$ (see Fig. 6) and the experimental observation that the intensity of satellite reflections for approximately the same value of $\sin\theta/\lambda$ do drop off monotonically and fairly sharply with increasing m, at the very most only 37 displacive degrees of freedom and 13 compositional degrees of freedom (9 if one assumes it is impossible to distinguish W from Ta) should ever be required to accurately describe the structure at any composition within the solid solution field. In the refinement of L-Ta_2O_5, however, some 90 displacive degrees of freedom

alone were refined (*11*). From a modulated structure point of view, there is clearly a rather large amount of over-parameterization involved in all the published structure refinements and hence the high degree of parameter interaction (blamed by Stephenson and Roth for the large esd's on the atomic coordinates) is not surprising. Furthermore, by resetting the published observed reflections (*8–11*) into the 4-index notation, it is clear that the number of observed reflections of the type $(hklm)^*$ diminish rapidly with increasing m. It follows that the compositional and displacive degrees of freedom associated with each harmonic order become less and less reliable as m increases. Refinement constraints like this can be easily built into a modulation wave approach to the structure refinement of such superstructures but not so easily into an isolated atom (or conventional space group) approach in which parameters on any one atom in the asymmetric unit are unrelated to parameters on any other atom in the asymmetric unit.

4.5. Possible Space Groups of Commensurate Phases

Given the superspace group symmetry of $P:Cmmm:s,-1,1$ along with the odd or even value of the prime integers in the fraction describing the rational value of $q = m/n$, three sets of possible space group symmetries (for the resultant $\mathbf{a}' = \mathbf{a}, \mathbf{b}' = n\mathbf{b}, \mathbf{c}' = \mathbf{c}$ cell) can occur. These three sets result from different choices for the global phase parameter ϕ. They are as follows:

$q = (2m + 1)/(2n + 1)$ (e.g. L-Ta_2O_5, where $q = \frac{7}{11}$ (*11*))

$\phi = 2J\,\pi/(4n + 2)$	$Pbam$
$\phi = (2J + 1)\,\pi/(4n + 2)$	$Pbmm$
$\phi =$ arbitrary	$Pb2_1m$.

Stephenson and Roth (*11*) refined the structure of L-Ta_2O_5, where $q = \frac{7}{11}$, in projection using the rectangular plane group pm. Given that the existence of a mirror perpendicular to **c** is always assumed to be present, the equivalent three-dimensional space group is $P2mm$.

$q = (2m + 1)/2n$ (e.g. $Ta_{30}W_2O_{81}$, where $q = \frac{5}{8}$ (*9*))

$\phi = 2J\,\pi/4n$	$Pbmm$
$\phi = (2J + 1)\,\pi/4n$	$Pbam$
$\phi =$ arbitrary	$Pb2_1m$.

Stephenson and Roth (*9*) refined the structure of $Ta_{30}W_2O_{81}$, where $q = \frac{5}{8}$, in projection using the rectangular plane groups pm and pg. The equivalent three-dimensional space groups are $P2mm$ and $Pb2_1m$, respectively.

$q = 2m/(2n + 1)$ (eg $Ta_{22}W_4O_{67}$, where $q = \frac{8}{13}$ (*8*))

$\phi = 2J\,\pi/(4n + 2)$	$C112/m$
$\phi = (2J + 1)\,\pi/(4n + 2)$	$C2mm$
$\phi =$ arbitrary	$C11m$.

Stephenson and Roth (*8*) refined the structure of $Ta_{22}W_4O_{67}$, where $q = \frac{8}{13}$, in projection using the rectangular plane group Cm. The equivalent three-dimensional space group is $C2mm$.

In all three cases above, J is an integer. In the first two cases, the different values of J simply correspond to different possible origin choices within the same structure. In the latter case, however, there are two different possible structures associated with the space group symmetry. The values of ϕ corresponding to these different possible structures are as follows:

$\phi = 0° + 4J\,\pi/(4n + 2)$	$C112/m$
$\phi = \pi + 4J\,\pi/(4n + 2)$	$C112/m$
$\phi = \pi/2 + 4J\,\pi/(4n + 2)$	$C2mm$

and

$\phi = -\pi/2 + 4J\,\pi/(4n + 2)$	$C2mm$.

Landau free-energy arguments suggest that an arbitrary choice of phase is highly unlikely (*18*) and that it is reasonable to assume that only the first two possible space groups in each case are relevant. The existence of so-called distortion planes as postulated by

Stephenson and Roth (*8–11*) is not, of necessity, required by the observed diffraction evidence although partial occupancies are e.g., a C-centred Bravais lattice for $Ta_{22}W_4O_{67}$ implies that some of the oxygen sites must be partially occupied. The diffraction symmetry is mmm for all the above possible values of ϕ even though the actual point group symmetry can be lower. Finally note that it would be rather difficult on refinement grounds alone to distinguish between these alternate choices of global phase. Thus the possibility of pseudo-homometry arises and it is conceivable that the published structure refinements correspond to false minima (*19–21*). Considerations other than refinement statistics alone are required to check chemical plausibility.

5. Apparent Valence Calculations

One of the most useful ways of checking the chemical plausibility of published structure refinements is via the calculation of apparent valences (AVs) using the bond length–bond valence approach (*22–24*). In this approach, the relationship between the length of a bond (r^{ij}) and its valence (s^{ij}) is written in the form $s^{ij} = \exp[(r_0^{ij} - r^{ij})/B]$, where r_0^{ij} and B are empirical parameters which can be refined via use of the Inorganic Crystal Structure Database (ICSD). The apparent valence (AV) of atom i, V_i', is then obtained as a sum over all the neighboring bond valences, i.e., $V_i' = \sum_j s^{ij}$. If these apparent valences are in reasonable accord (i.e., within ± 0.2 valence units) of the theoretically expected valences (in our case we would expect a valence of 5 for Ta, 6 for W, and 2 for O) one can have confidence that the structure has been reliably determined. Brown and Altermatt (*23*) have refined the parameters r_0^{ij} and B for over 750 atom pairs and listed the 141 most accurately determined values for r_0^{ij}. They find empirically that B can be set to a constant—namely 0.37 Å. By the calculation of apparent valences (AVs) (*4*) for the (closely related) reported crystal structure of $Zr_7O_9F_{10}$ (*3*), for example, it has recently proved possible not only to confirm the chemical plausibility of the published structure but also to identify those anion sites which are occupied by O, those occupied by F, and those sites occupied by a mixture of O and F.

In the case of the $Ta_2O_5 \cdot WO_3$ (from 0 to ~27 mol.% WO_3) system, a similar problem arises due to the similar X-ray scattering curves of Ta and W. Hence Stephenson and Roth (*8–11*) were not able to determine whether Ta and W atoms were ordered or disordered. Although all four of the published structure refinements (*8–11*) within the $Ta_2O_5 \cdot WO_3$ (from 0 to ~27 mol.% WO_3) composition range gave very large e.s.d's (~ ±0.2 Å) for the atomic coordinates, it is nonetheless instructive to use the bond length–bond valence approach to check their plausibility and to look for any tendency for Ta, W ordering. As discussed in the paper reporting the structure refinement of $Ta_{22}W_4O_{67}$ (*8*), neighboring O(17) sites related by the mirror plane perpendicular to **b** are too close to be simultaneously occupied as are neighboring O(17) and O(18) sites. Hence these sites are only partially occupied, i.e., atom O(18) has an occupancy of ½ while atom O(17) has one of ¼. The *C*2*mm* space group symmetry is then compatible with the stoichiometry of $Ta_{22}W_4O_{67}$. In calculating apparent valences it is important to use the local coordination rather than the average coordination. Hence the different coordinations resulting from these partial occupancies were taken into account.

Table II presents the Apparent Valences (AVs) for the reported crystal structure refinement of $Ta_{22}W_4O_{67}$ (*8*). There are clearly very major problems with the refinement from the point of view of AV's. Many atoms are substantially over- or under-bonded, e.g., *M*(1), *M*(2), *M*(4), *M*(7'), O(1), O(3), O(5), O(7), O(8), and O(9). What is unclear,

TABLE II

APPARENT VALENCES[a,b] FOR $Ta_{22}W_4O_{67}$

Atom	AV		Atom	AV	
	All Ta	All W		All Ta	All W
M(1)	4.49	4.26	O(1)	2.56	2.43
M(1′)	5.30	5.02	O(2)	2.10	1.99
M(2)	6.82	6.47	O(3)	1.69	1.60
M(2′)	6.10	5.77	O(4)	1.91	1.87
M(2″)	6.03	5.71	O(5)	2.60	2.46
M(3)	6.04	5.72	O(6)	2.17	2.05
M(4)	6.79	6.44	O(7)	2.62	2.48
M(5)	4.95	4.69	O(8)	2.95	2.80
M(6)	4.94	4.68	O(9)	2.86	2.71
M(7)	5.22	4.95	O(10)	1.77	1.68
M(7′)	5.49	5.20	O(11)	1.98	1.88
M(7″)	4.71	4.46	O(12)	1.93	1.82
			O(13)	1.99	1.89
			O(14)	2.00	1.89
			O(15)	2.00	1.89
			O(16)	2.00	1.89
			O(17)	2.81	2.67
			O(18)	2.30	2.18
			O(19)	1.94	1.84

[a] Using bond valence parameters R_0 (Ta–O) = 1.920 Å and R_0 (W–O) = 1.900 Å.

[b] Note that there exist two distinct possible coordinations for the *M*(1) site (labeled *M*(1) and *M*(1′)), three distinct possible coordinations for the *M*(2) site (labeled *M*(2), *M*(2′), and *M*(2″)), and three distinct possible coordinations for the *M*(7) site (labeled *M*(7), *M*(7′), and *M*(7″)). The columns labelled "All Ta" and "All W" correspond to the AVs obtained if all metal atom sites are presumed to be occupied by Ta and W, respectively.

however, is whether or not the AVs can be made more satisfactory via an adjustment of atomic coordinates compatible with the large (~ ±0.2 Å) e.s.d's given for each atomic coordinate, or whether it might be that these refinements represent false minima due to an incorrect choice of global phase as discussed above. The agreement between AVs and theoretically expected valences are no better for any of the other published crystal structure refinements. It is clear that none of these structures are chemically or crystallographically plausible.

6. Interpretation of the Range of Solid Solution and the Diffuse Intensity Distributions

As in the recent study of the structurally related $ZrO_{2-x}F_{2x}$ it was helpful to use bond valence calculations to try to understand both the range of this solid solution, $(1 - x)Ta_2O_5 \cdot xWO_3$ $0.0 \leq x \leq 0.267$, and the diffuse intensity distribution observed via TEM.

Firstly, the range of solid solution can be understood if we consider all the bonding and non-bonding interactions in the system. Experimentally we observe (Fig. 4) that the parent unit cell dimensions in absolute terms vary little across the solid-solution, and for our purpose we consider them to be constant and ideal i.e., $\sqrt{3}\mathbf{a} = \mathbf{b}$. When we consider the α-UO_3-type parent structure the coordination (or bonding environment) of the cation is 6 + 2 (hexagonal bipyramid), the apical anion, A_1, is in twofold coordination and the equatorial anions, A_2 and A_3, are in threefold coordination. In $(1 - x)Ta_2O_5 \cdot xWO_3$, which we describe as an anion-

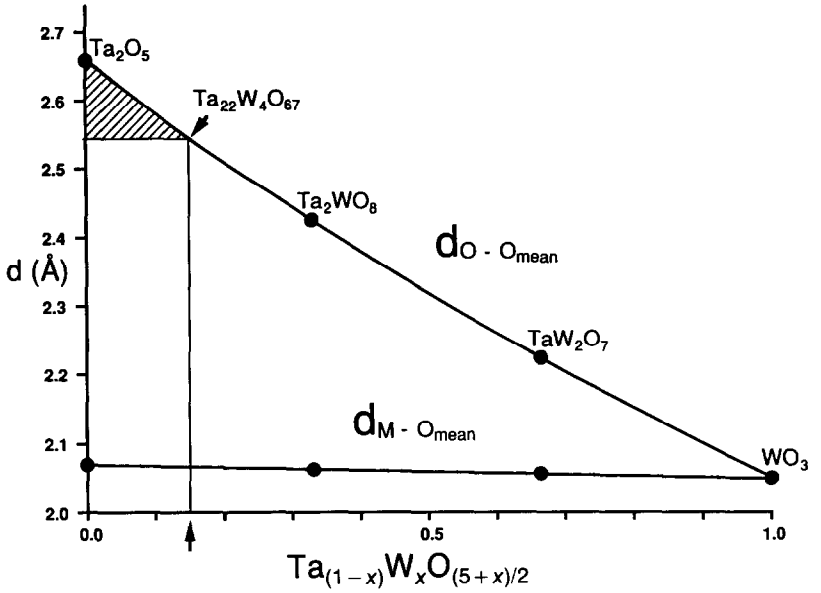

FIG. 8. Plot of the average $d_{(O-O)}$ in the "circumference" of an idealized metal–oxygen polyhedron versus the composition of $Ta_{(1-x)}W_xO_{(5+x)/2}$ with $0 \leq x \leq 1$.

deficient α-UO_3-type, if we assume that the bonding requirements of the apical oxygen are satisfied, i.e., its AV is exactly 2.0, then in order to satisfy the bonding requirement of the cation the remaining bond valence contribution, or bond order, of each M–O bond must be $\frac{2}{3}$ on average. This follows likewise in that each equatorial oxygen is three-coordinate and must sum to 2.0. When M = W there will be six such equatorial M–O bonds, when $M = Ta_{0.333}W_{0.667}$ (on average) there will be 5.5 such M–O bonds, when $M = Ta_{0.667}W_{0.333}$ (on average) there will be five (analogous to the α-U_3O_8 structure) and when M = Ta there will be 4.5. The average M–O distance is necessarily determined by the bond valence requirement of the cation. If we then idealize the n-gonal bipyramid for each of these compositions we can calculate what the average $d_{(O-O)}$ is on the 'circumference' of this polyhedron. We have plotted these results in Fig. 8. The most anion-deficient composition observed for $(1 - x)Ta_2O_5 \cdot xWO_3$ occurs when $x = 0.267$, i.e., $Ta_{22}W_4O_{67}$. This composition corresponds to an average $d_{(O-O)}$ of 2.55 Å, which compares with closest O–O contacts of 2.51 Å in $Zr_7O_9F_{10}$, 2.57 Å in α-U_3O_8, and 2.58 Å in baddeleyite (see Ref. (*4*)). Thus it would appear that nonbonding O–O contacts in $(1 - x)Ta_2O_5 \cdot xWO_3$ determine the lower limit of oxygen vacancies required by this structure for this system. The upper limit is simply determined by the end member, namely Ta_2O_5.

Secondly, the diffuse intensity distribution shown in Figs. 5b and d and described in Section 3.4 can also be understood in bond valence terms. As the apical oxygen atoms are two coordinate one can determine the magnitude of the **c** axis if one requires the bond valence of those oxygens to be exactly 2.0. As there is no evidence for ordering of Ta and W along an –M–O–M–O– string parallel to **c** we can determine the average **c** axis dimension assuming a random distribution in that direction. These values are plotted in Fig. 9 for all composi-

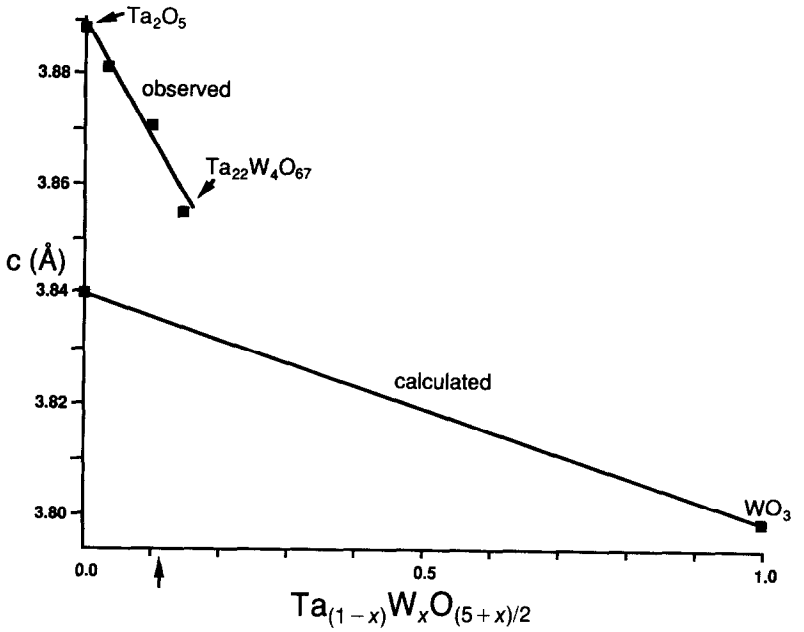

FIG. 9. Plot of the calculated and observed **c** axis dimension versus the compostion of $Ta_{(1-x)}W_xO_{(5+x)/2}$ with $0 \leq x \leq 1$. The calculated values are on the basis of AVs assuming a random distribution of Ta and W along the $-M-O-M-O-$ chains along **c**. The observed values appear to be about 1% greater than the calculated dimensions.

tions together with the observed **c** dimensions. It is striking that the observed dimensions are ~1% greater than the calculated dimensions. Of course, these calculated values assume that both the metal atoms and the apical oxygen atoms lie on the mirror planes perpendicular to **c**. If we allow either the oxygen or metal to move off the mirror, while still constraining the bond valence of the oxygen to be 2.0, the result is an increase in the calculated *c* dimension. This is because the bond length–bond valence relationship is exponential. The relationship between the offset from the mirror plane, Δd, and the **c** axis increase, $\Delta \mathbf{c}$, is shown in Fig. 10. To obtain a 1% increase in the c dimension would require a 0.14 Å offset. This motion would be consistent with the diffuse intensity distribution observed via electron diffraction which requires correlated atomic motion approximately parallel to **c** with the displacements of neighboring $-M-O-M-O-$ chains completely uncorrelated.

7. Conclusion

We have shown in this study that the series of compounds $(1 - x)Ta_2O_5 \cdot xWO_3$ in the range $0 \leq x \leq 0.267$ is best described as a solid solution with a single incommensurately modulated structure, with primary modulation wave vector varying continuously as a function of composition. While the earlier description by Roth and Stephenson, namely an infinite series of line phases is not necessarily incorrect, our modulated structure description has the distinct advantage of requiring only one space group to describe all the compositions.

Consideration of the AVs for the four

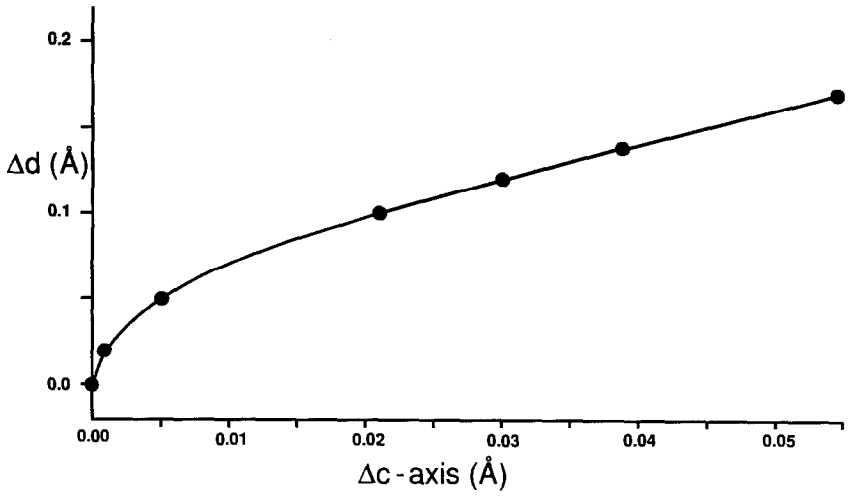

FIG. 10. Plot of the required offset Δd of the atoms from the mirror planes perpendicular to **c** versus the increase Δc of the **c** axis.

reported $(1 - x)Ta_2O_5 \cdot xWO_3$ structures suggests that all are chemically implausible, though the authors of that work did acknowledge that there were such problems in their refined structural models. Similar AV calculations on an idealized parent structure have enabled us to identify nonbonded O–O interactions as the limiting factor on the anion-rich end of the range, namely $x = 0.267$.

Due to the deficiencies of the earlier single crystal X-ray structure refinements we are currently attempting to improve on those refinements using a modulated structure approach.

Acknowledgments

The authors thank Professor A. D. Rae for fruitful discussions during the writing of the present paper, Professor M. O'Keeffe for the program EUTAX used to calculate the Apparent Valences, and Mr. K. Owen for assistence with the densitometer traces.

References

1. L. JAHNBERG AND S. ANDERSSON, *Acta Chem. Scand.* **21,** 615 (1967).
2. R. PAPIERNIK, B. FRIT, AND B. GAUDREAU, *Rev. Chim. Min.* **23,** 400 (1986).
3. B. HOLMBERG, *Acta Crystallogr Sect. B* **26,** 830 (1970).
4. J. G. THOMPSON, R. L. WITHERS, AND C. J. KEPERT, *J Solid State Chem.* **95,** 111 (1991).
5. R. S. ROTH AND N. C. STEPHENSON, *in* "Chemistry of Extended Defects in Non-Metallic Solids" (L. Eyring and M. O'Keeffe, Eds.), pp. 167–182, North-Holland, Amsterdam (1970).
6. R. S. ROTH, J. L. WARING, AND H. S. PARKER, *J. Solid State Chem.* **2,** 445 (1970).
7. J. M. WILLIAMS. R. J. D. TILLEY, G. HARBURN, AND R. P. WILLIAMS, *J. Solid State Chem.* **92,** 460 (1991).
8. N. C. STEPHENSON AND R. S. ROTH, *Acta Crystallogr. Sect. B* **27,** 1010 (1971).
9. N. C. STEPHENSON AND R. S. ROTH, *Acta Crystallogr. Sect. B* **27,** 1018 (1971).
10. N. C. STEPHENSON AND R. S. ROTH, *Acta Crystallogr. Sect. B* **27,** 1031 (1971).
11. N. C. STEPHENSON AND R. S. ROTH, *Acta Crystallogr. Sect. B* **27,** 1037 (1971).
12. J. M. PÉREZ-MATO, F. GAXTELUA, G. MADARIAGA, AND M. J. TELLO, *J. Phys. C* **19,** 1923 (1986).
13. B. E. WARREN, B. L. AVERBACH, AND B. W. ROBERTS, *J. Appl. Phys.* **22,** 1493 (1951).
14. T. R. WELBERRY, *J. Appl. Crystallogr.* **19,** 382 (1986).
15. P. M. DE WOLFF, T. JANSSEN, AND A. JANNER, *Acta Crystallogr. Sect. A* **37,** 625 (1981).
16. C. J. BRADLEY AND A. P. CRACKNELL, "The Mathematical Theory of Symmetry in Solids," Clarendon Press, Oxford 1972.
17. J. M. PÉREZ-MATO, G. MADARIAGA, F. J. ZUÑIGA,

AND A. GARCIA ARRIBAS, *Acta Crystallogr. Sect. A* **43,** 216 (1987).
18. J. M. PÉREZ-MATO, *Solid State Commun.* **67,** 1145 (1988).
19. J. G. THOMPSON, A. D. RAE, R. L. WITHERS, T. R. WELBERRY, AND A. C. WILLIS, *J. Phys. C* **21,** 4007 (1988).
20. A. D. RAE, J. G. THOMPSON, R. L. WITHERS, AND A. C. WILLIS, *Acta Crystallogr. Sect. B* **46,** 474 (1990).
21. A. D. RAE, J. G. THOMPSON, AND R. L. WITHERS, *Acta Crystallogr. Sect. B* **47,** 870 (1991).
22. I. D. BROWN, *Chem. Soc. Rev.* **7,** 359 (1978).
23. I. D. BROWN AND D. ALTERMATT, *Acta Crystallogr. Sect. B* **41,** 244 (1985).
24. M. O'KEEFFE, *Struct. Bonding* **71,** 161 (1989).